Materials Transactions, Vol. 56, No. 4 (2015) pp. 570 to 575

In-Beam Stress Corrosion Behavior of Welded 308 Stainless Steel at 473 K in Aerated and Hydrogenated Water Conditions

Yoshiharu Murase*, Norikazu Yamamoto, Tadashi Shinohara, Akira Tahara and Kazuhiro Kimura

National Institute for Materials Science, Tsukuba 305-0047, Japan

Stress corrosion tests were performed for welded 308 stainless steel under proton irradiation at 473 K in aerated water (DO: 0.15–0.22 ppm, DH: <10 ppb) and hydrogenated water (DH: 1.0–1.4 ppm, DO: <5 ppb) conditions. The in-beam loading condition was 0 and 300 MPa in tension under an irradiation dose rate of 1.3×10^{-7} dpa/s. In situ measurement of electrochemical corrosion potential (ECP) and subsequent SEM analysis were also conducted for all the specimens. In the aerated water condition, the process of stress corrosion cracking (SCC) was significantly accelerated under irradiation, while the in-beam effect on SCC was suppressed in the hydrogenated water condition. The in-beam stress corrosion behavior is discussed in terms of both water radiolysis and radiation-induced microstructures.
[doi:10.2320/matertrans.MBW201404]

(Received October 21, 2014; Accepted January 20, 2015; Published February 27, 2015)

Keywords: *welded stainless steel, stress corrosion cracking, proton irradiation, corrosion pit, radiolysis, dissolved gas*

1. Introduction

The degradation of resistance to stress corrosion cracking (SCC) at welded joints is a major concern for the use of stainless steel structural materials in a corrosive environment. A cast structure with delta ferrite phases in the austenitic matrix designed to prevent hot-cracking during weld metal solidification in the weld metal zone can enhance the susceptibility to pitting corrosion at the boundaries of delta ferrite phases.[1,2] Preferential formation of corrosion pits and subsequent initiation of SCC along the boundaries have been discussed in terms of the deterioration of passive film due to the depletion of chromium[3] or mismatch of lattice structures[4] at the boundaries. Some authors have pointed out that the selective dissolution of delta ferrite phases in the electrochemical reactions can lead to the initiation of SCC.[5] Besides these metallurgical factors, it is well accepted that neutron irradiation can significantly modify SCC behavior through radiolysis of coolant water and microstructural/microchemical changes in materials produced by displacement damage. In particular, radiolysis products such as hydroperoxy and other radical species are considered to induce additional corrosive attacks on stainless steels used for nuclear reactors or containers of nuclear waste. For the purpose of suppressing water radiolysis, the addition of hydrogen to the primary cooling water has been widely used for the core materials of nuclear reactors.[6]

In our previous study,[7] stress corrosion tests in pure water at 473 K were conducted under 17 MeV proton irradiation for welded 308 stainless steel in order to investigate the in-beam effect on the formation of corrosion pits which lead to the initiation of SCC at the weld metal. It was concluded that extensive electrochemical reactions at the stress-induced defects in the passive film with radiolysis products would cause the initiation of SCC along the boundaries of delta ferrite phases in the in-beam stress specimens. However, the in-beam SCC behavior in practical water conditions remained to be examined as the next step of our study. In the present study, we conducted in-beam stress corrosion tests of welded 308 stainless steels in hydrogenated and aerated water at 473 K, in order to clarify the effects of dissolved hydrogen (DH) and oxygen (DO) on in-beam SCC behavior at the weld metal.

*Corresponding author, E-mail: murase.yoshiharu@nims.go.jp

Table 1 Chemical composition of SUS308.

	Ni	Cr	Mn	V	C	Si	P	S	Fe
308	10.55	19.05	1.73	0.064	0.02	0.23	0.026	0.004	Balance

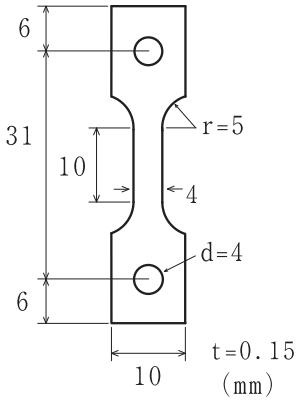

Fig. 1 Specimen preparation for SCC test.

2. Experimental Procedure

The material used in the present study was welded 308 stainless steel. The chemical composition of the material is shown in Table 1. The material was sliced and punched-out into the specimen as shown in Fig. 1. The specimen was mechanically ground to a thickness of 0.14 mm and then polished to a mirror finish for the stress corrosion tests. The tensile strength (TS) and 0.2% yield stress (0.2% YS) of the specimens at 473 K were 400 ± 20 MPa and 320 ± 20 MPa on average with error range, respectively.

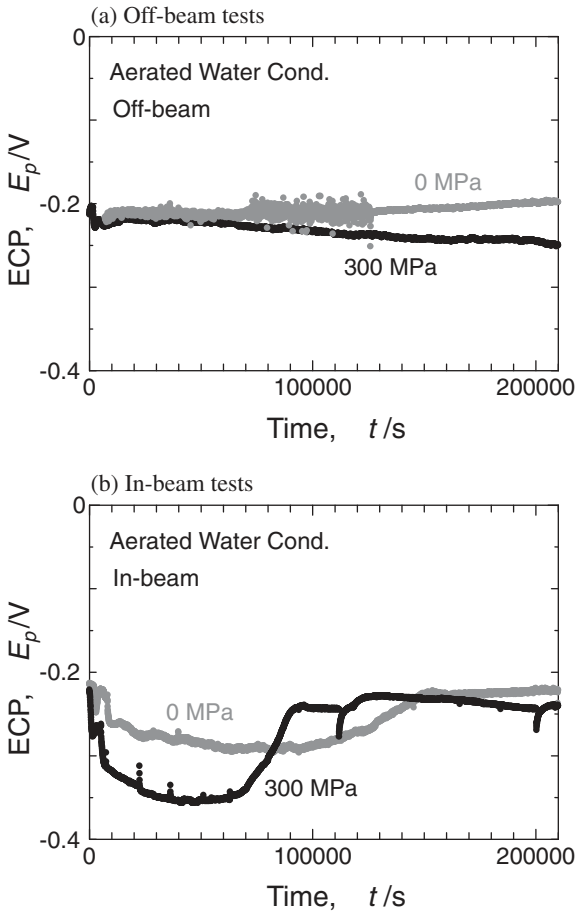

Fig. 2 Plots of ECP as a function of time for (a) off-beam and (b) in-beam corrosion tests in the aerated water condition.

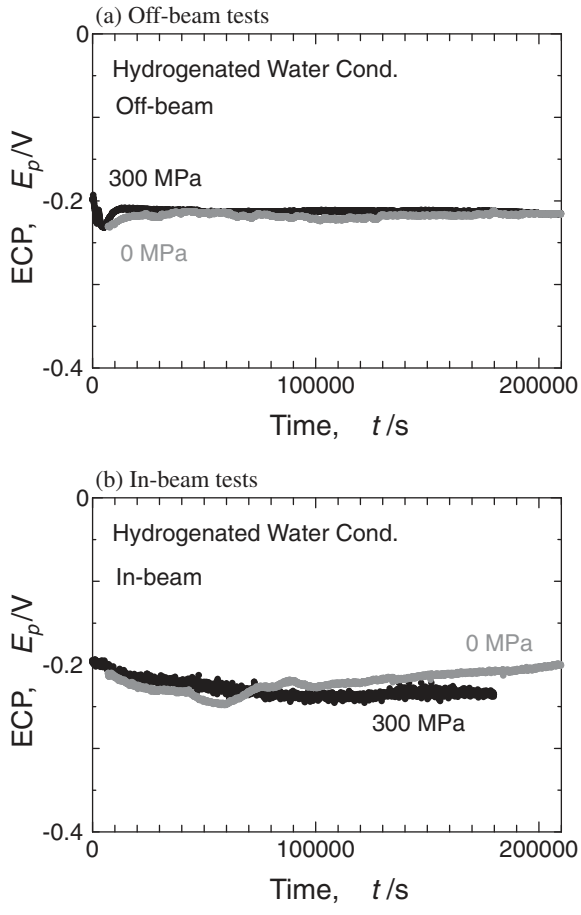

Fig. 3 Plots of ECP as a function of time for (a) off-beam and (b) in-beam corrosion tests in the hydrogenated water condition.

The in-beam stress corrosion tests were conducted in aerated water and hydrogenated water conditions at 473 K for 2.16×10^5 s. The concentration of DO and DH was controlled to be 0.15–0.22 ppm and <10 ppb in the aerated water condition, and 1.0–1.4 ppm and <5 ppb in the hydrogenated water condition, respectively. The loading stress on the specimen gauge was adjusted to 0 and 300 MPa. The proton beam intensity was set to 1.0 μA/cm^2, corresponding to the displacement damage rate of 1.3×10^{-7} dpa/s on average for the specimen. As a control, off-beam tests were also conducted under the same conditions. In situ measurement of electrochemical corrosion potential (ECP) was carried out for all the tests. Since the in-beam specimen at 300 MPa in the aerated water condition fractured during the test for 2.16×10^5 s, an additional in-beam test at 300 MPa was conducted for 1.08×10^5 s in the same water condition. The fracture surface of the in-beam specimen was examined by scanning electron microscopy (SEM, JEOL5310). As for the other specimens, the oxide layer on the specimen surface was surveyed by SEM, and the density of corrosion pits was measured over a surface area of 129.4×96.2 μm^2. Details of the welding conditions, specimen preparation and in-beam stress corrosion apparatus are described elsewhere.[7,8]

3. Results

Figures 2 and 3 show the plots of ECP as a function of time for (a) off-beam and (b) in-beam tests at 0 and 300 MPa in aerated and hydrogenated water conditions, respectively. In the aerated water condition, ECP plots were mostly stable in the range from −0.20 to −0.22 V during the off-beam tests at 0 MPa, whereas ECP gradually decreased for the off-beam specimen at 300 MPa (see Fig. 2(a)). As for the in-beam tests shown in Fig. 2(b), the plots shifted steeply from −0.22 to −0.30 V and then gradually back to −0.22 V during the tests at 0 MPa, while a similar shift but more drastic decrease and recovery of ECP between −0.22 and −0.35 V was observed for the test at 300 MPa. As a result of the in-beam stress corrosion test at 300 MPa in the aerated water condition, the specimen fractured within 2.16×10^5 s. The lifetime to fracture is estimated to be in the range between 1.08×10^5 and 2.16×10^5 s, because the specimen did not fracture in the additional in-beam test at 300 MPa for 1.08×10^5 s in the aerated water condition. In the hydrogenated water condition, ECP was almost constant at −0.22 V during the off-beam tests at 0 and 300 MPa (see Fig. 3(a)). A slight decrease of ECP from −0.20 to −0.24 V was detected during the in-beam tests at 0 and 300 MPa, and then a subsequent recovery to −0.20 V was observed for the test at 0 MPa while staying at −0.24 V for 300 MPa, as shown in Fig. 3(b).

Typical specimen surfaces after the stress corrosion tests are displayed in Figs. 4 and 5 for the off-beam specimens at (a) 0 MPa and (b) 300 MPa, and for the in-beam specimens at (c) 0 MPa and (d) 300 MPa in the aerated and hydrogenated

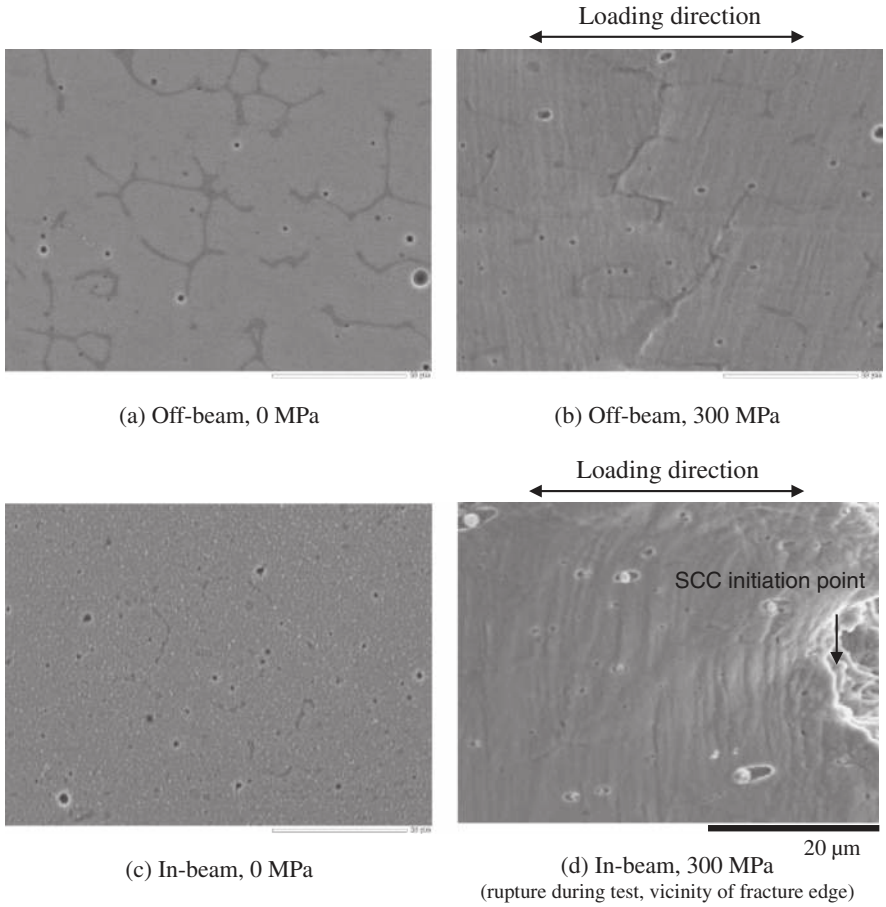

Fig. 4 SEM photos of surface oxide layer for off-beam specimens at (a) 0 MPa and (b) 300 MPa, for in-beam specimens at (c) 0 MPa and (d) 300 MPa in the aerated water condition.

water condition, respectively. As for the specimen that fractured during the in-beam test at 300 MPa in the aerated water condition, the specimen surface in the vicinity of the fracture edge is presented in Fig. 4(d). The formation of corrosion pits on the surface was detected for all the specimens. Most of the corrosion pits appeared to form at the boundaries of delta ferrite phases in the austenite matrix. Table 2 summarizes the density of corrosion pits on the surface for each specimen. In the aerated water condition, the initiation of surface cracking along the boundaries of delta ferrite phases was observed for the off-beam specimen at 300 MPa, as shown in Fig. 4(b). A substantial increase in the density of corrosion pits was detected for the in-beam specimen at 0 MPa (see Fig. 4(c) and Table 2). Severe plastic deformation with secondary cracks occurred at the surface for the in-beam specimen at 300 MPa that fractured during the test, as shown in Fig. 4(d). However, in the hydrogenated water condition, similar density measurements of corrosion pits without any signs of crack initiation were obtained for all the specimens (see Table 2 and Fig. 5). Figure 6 shows SEM photos of the fracture surface for the in-beam specimen at 300 MPa in the aerated water condition. The fractographic morphology of the fracture surface was mostly characterized by glide plane decohesion and dimples, with an indication of transgranular cracking in the ductile fracture mode. However, at the initiation point of SCC, some quasi-cleavage steps with fewer dimples on their planes implied active path corrosion at the initial stage of SCC.

4. Discussion

It is well documented that in situ monitoring of ECP is a useful way to estimate the evolution of electrochemical reactions on metal surfaces. The electrochemical reactions are represented as the following anodic and cathodic reactions, respectively:

$$M \rightarrow M^{n+} + ne^- \quad \text{(anodic reaction)} \quad (1)$$

$$O_2 + 4e^- + 2H_2O \rightarrow 4OH^- \quad \text{(cathodic reaction)} \quad (2)$$

where M is a metal element, and n is the valence number of M. According to the Evans diagram (ECP vs. log (corrosion current "i_{corr}")), ECP corresponds to the potential at the crossing point of Tafel plots for anodic/cathodic reactions.[9,10] The value of $\log i_{corr}$ at the crossing point directly reflects the corrosion rate. Figure 7 shows the schematic Evans diagrams indicating the possible variations of ECP and i_{corr} (corrosion current) in several situations. The diagram shown in Fig. 7(a) presents the Tafel plots in the initial situation where anodic/cathodic reactions are balanced prior to the in-beam stress corrosion test. When the cathodic reaction is more enhanced than the anodic reaction (Δcathodic $>$ Δanodic $>$ 0), both ECP and i_{corr} increase as shown in Fig. 7(b), while a more enhanced anodic than cathodic reaction (Δanodic $>$ Δcathodic $>$ 0) leads to an increase of i_{corr} but a decrease of ECP, as shown in Fig. 7(c). The decrease in anodic reaction (Δanodic $<$ 0) due to the formation of passive film on the metal surface results in a

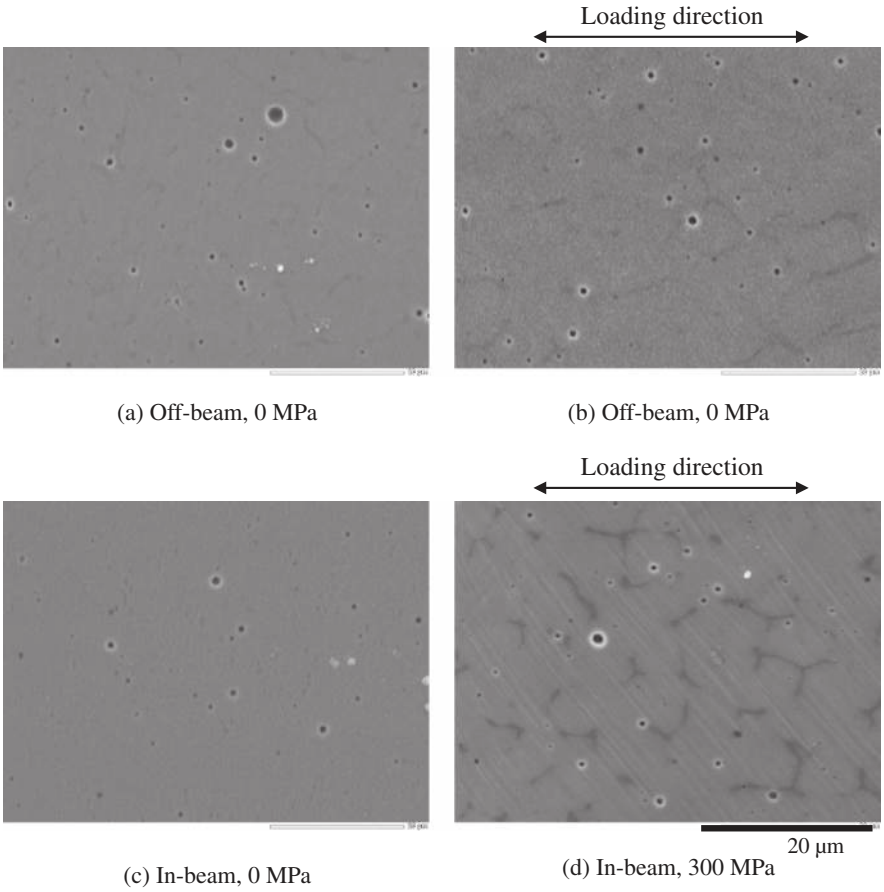

Fig. 5 SEM photos of surface oxide layer for off-beam specimens at (a) 0 MPa and (b) 300 MPa, for in-beam specimens at (c) 0 MPa and (d) 300 MPa in the hydrogenated water condition.

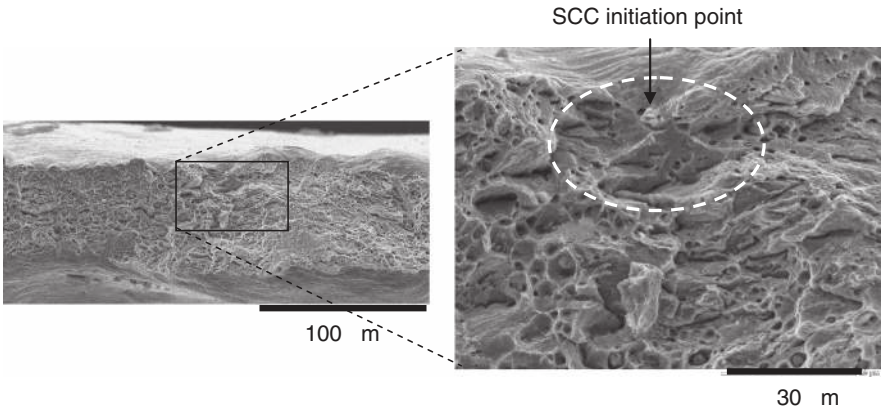

Fig. 6 SEM photos of fracture surface in the vicinity of SCC initiation point for in-beam specimen at 300 MPa in the aerated water condition.

Table 2 Density of corrosion pits on SCC specimens.

Beam and stress conditions	Aerated water condition	Hydrogenated water condition
	Density (cm^{-2})	Density (cm^{-2})
Off-beam, 0 MPa	7.7×10^5	9.6×10^5
Off-beam, 300 MPa	8.5×10^5	8.6×10^5
In-beam, 0 MPa	1.1×10^6	1.0×10^6
In-beam, 300 MPa	6.8×10^5 (rupture during test)	9.3×10^5

decrease of i_{corr} but an increase of ECP (see Fig. 7(d)). The influence of water radiolysis on electrochemical reactions has been investigated under in situ irradiation conditions in light water reactors[9,10] and ion accelerators.[11–14] Since some radiolysis products such as oxygen, hydrogen peroxide and other radicals can act as strong oxidants in a water solution, the reduction reactions of oxidant species, namely cathodic reactions, are mainly enhanced by water radiolysis.[9,11] The addition of hydrogen to the water environment is well recognized as an effective countermeasure to suppress water radiolysis.[6] A drastic decrease in the production density of

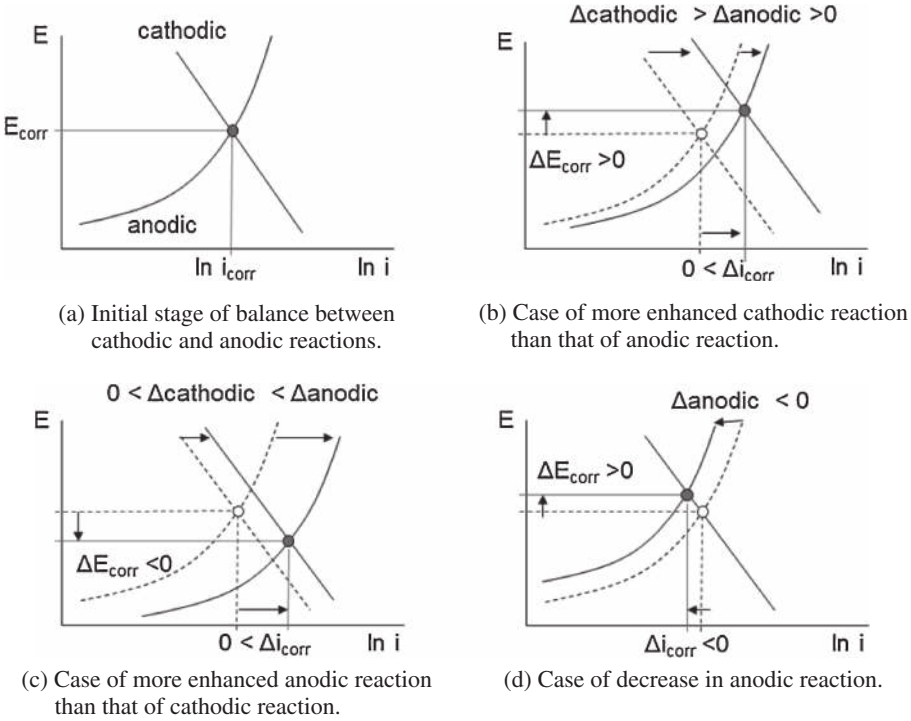

(a) Initial stage of balance between cathodic and anodic reactions.

(b) Case of more enhanced cathodic reaction than that of anodic reaction.

(c) Case of more enhanced anodic reaction than that of cathodic reaction.

(d) Case of decrease in anodic reaction.

Fig. 7 Schematic Evans diagrams indicating possible variations of ECP and i_{corr} (corrosion current) from (a) initial stage to the stages of (b) more enhanced cathodic reaction than that of anodic reaction, (c) more enhanced anodic reaction than cathodic reaction and (d) decrease in anodic reaction.

radiolysis oxidant species as a function of DH concentration has been reported in an in-pile reactor environment.[9] A recent report of in-beam corrosion tests has also demonstrated the decrease of DO concentration during tests in the hydrogenated water condition.[13] In addition to water radiolysis, the microstructure changes in the materials produced by displacement damage would be a factor affecting the electrochemical reactions. Since a higher diffusion rate of oxygen along dislocations than that in the matrix has been pointed out for stainless steels,[15] the development of dislocation structures under irradiation could provide additional internal areas to be oxidized, and thereby contribute to the increase of anodic reaction.

In the present experiments, a gradual decrease of ECP for the specimen was detected for the off-beam specimen at 300 MPa in the aerated water condition, as shown in Fig. 2(a). This indicates a slight promotion of additional anodic reactions at the microdefects induced by stress on the passive film, resulting in crack initiation along the boundaries of delta ferrite phases (see Fig. 4(b)). The decrease and recovery of ECP during the in-beam test at 0 MPa, as shown in Fig. 2(b), reflects a transient promotion of electrochemical reactions until the formation of the passive film. A flash increase of reactions seemed sufficient to cause a substantial increase in the density of corrosion pits (see Table 2). As presented in Fig. 7(b), the decrease of ECP could not be explained by only the enhanced cathodic reaction due to water radiolysis. Therefore, a significant enhancement of anodic reaction due to the development of dislocation structures under irradiation would contribute to a transient decrease of ECP (see Fig. 7(c)) for the in-beam test at 0 MPa. A similar behavior but more drastic change of ECP was detected for the in-beam tests at 300 MPa, as shown in Fig. 2(b). Besides the promoted electrochemical reactions under irradiation, the additional anodic reactions at the microdefects induced by stress would accelerate the process of SCC along the boundaries of delta ferrite phases on the specimen surface. Quasi-cleavage steps at the initiation point of SCC on the fracture surface shown in Fig. 6(b) also support active path corrosion along the boundaries in the initial process of SCC. In comparison with the crack initiation for the in-beam specimen at 300 MPa in pure water in the previous study,[7] the specimen completely fractured during the in-beam tests at 300 MPa in the present aerated water condition. Thus, the process of SCC would be significantly accelerated under irradiation in the aerated water condition.

On the other hand, as shown in Fig. 5 and Table 2, similar density of corrosion pits without any signs of crack initiation was detected for all the specimens in the hydrogenated water condition. These results indicate that both stress and irradiation are no longer effective for modifying the corrosion rate in this water condition. Similar ECP behavior for off-beam tests with 0 and 300 MPa (see Fig. 3(a)) implies the suppression of additional anodic reaction at the microdefects induced by stress on the passive film for the test at 300 MPa. The addition of hydrogen would play a role in effectively reducing the concentration of DO at the microdefects. A slight decrease of ECP for in-beam tests (see Fig. 3(b)) indicates some increase of anodic reaction due to the development of dislocation structures under irradiation. However, due to the suppression of water radiolysis, the concentration of DO and other oxidant species would become too small to modify the corrosion behavior for in-beam

specimens. Therefore, the in-beam effect on SCC behavior would be suppressed in the hydrogenated water condition.

The decrease of ECP under proton irradiation has been reported to be correlated to the irradiation temperature, namely the obvious drop of ECP below 473 K but no ECP change between 523 and 573 K.[12] The authors[12] have attempted to explain the temperature dependence of the ECP drop with respect to the kinetics constants of electrochemical reactions of the radiolysis species, which follow the Arrhenius law. Furthermore, from the general viewpoint of radiation-induced microstructures at temperatures below 573 K,[16] the higher nucleation rate of interstitial dislocation loops would lead to a sufficiently higher dislocation density to enhance anodic reactions at an earlier stage of irradiation. Since the promotion of in-beam effect on SCC behavior related to the decrease of ECP was demonstrated in the present experiments, the present results would contribute to the understanding of SCC behavior for structural materials operated under irradiation at temperatures below 473 K.

5. Conclusion

Stress corrosion tests in aerated and hydrogenated water conditions were performed under 17 MeV proton irradiation for welded 308 stainless steel at 473 K. From the experimental results of in-beam and off-beam tests at 0 and 300 MPa, the following conclusions were drawn:

(1) In the aerated water condition, plots of ECP were mostly stable during the off-beam tests at 0 MPa, whereas a gradual decrease of ECP was observed for the off-beam specimen at 300 MPa. The initiation of surface cracking along the boundaries of delta ferrite phases was observed for the off-beam specimen at 300 MPa. As for the in-beam specimens, the decrease and recovery of ECP was detected during the test at 0 MPa, and a similar behavior but more drastic change of ECP was observed for the test at 300 MPa. A substantial increase in the density of corrosion pits was detected for the in-beam specimen at 0 MPa. Severe plastic deformation with secondary cracks occurred on the surface in the vicinity of the fracture edge for the in-beam specimen at 300 MPa that fractured during the test. Some quasi-cleavage steps with fewer dimples were detected on the fracture surface at the initiation point of SCC for the in-beam specimen at 300 MPa.

(2) In the hydrogenated water condition, ECP was almost constant during the off-beam tests at 0 and 300 MPa. A slight decrease of ECP was detected during the in-beam tests at 0 and 300 MPa, and a subsequent recovery was observed during the test at 0 MPa. A less significant difference in not only the pit density but also the appearance of the specimen surface was detected for all the specimens.

(3) Although the process of SCC would be significantly accelerated under irradiation in the aerated water condition, the in-beam effect on SCC behavior would be suppressed in the hydrogenated water condition. In the present study, the in-beam effect on SCC was discussed in terms of not only water radiolysis but also radiation-induced microstructures. The present experimental results would contribute to the understanding of SCC behavior for structural materials operated under irradiation at temperatures below 473 K.

Acknowledgement

We thank Dr. Hiromichi Hongo, NIMS, for providing the welded materials and technical support for specimen preparation.

REFERENCES

1) B. T. Lu, Z. K. Chen, J. L. Luo, B. M. Patchett and Z. H. Xu: Electrochim. Acta **50** (2005) 1391–1403.
2) H. Shaikh, H. S. Khatak, S. K. Seshadri, J. B. Gnanamoorthy and P. Rodriguez: Metall. Mater. Trans. A **26** (1995) 1859–1868.
3) K. S. Raja and K. P. Rao: Corrosion **51** (1995) 586–592.
4) G. M. Reddy, K. S. Rao and T. Sekhar: Sci. Tech. Weld. Join. **13** (2008) 363–377.
5) Z. Fang, Y. Wu and R. Zhu: Corrosion **50** (1994) 171–175.
6) D. D. Macdonald: Corrosion **48** (1992) 194–205.
7) Y. Murase, N. Yamamoto, T. Shinohara, A. Tahara, T. Ogata and K. Kimura: Mater. Trans. **55** (2014) 1445–1450.
8) M. Yamazaki, Y. Monma, H. Hongo, T. Watanabe, J. Kinugawa and Y. Muramatsu: Trans. NRIM **33** (1991) 64–71.
9) H. Takiguchi, M. Ullberg and S. Uchida: J. Nucl. Sci. Technol. **41** (2004) 601–609.
10) R. W. Bosch, M. Weber and M. Vankeerberghen: J. Nucl. Mater. **360** (2007) 304–314.
11) E. Leoni, C. Corbel, V. Cobut, D. Simon, D. Feron, M. Roy and O. Raquet: Electrochem. Acta **53** (2007) 495–510.
12) B. Muzeau, S. Perrin, C. Corbel, D. Simon and D. Feron: J. Nucl. Mater. **419** (2011) 241–247.
13) S. S. Raiman, A. Flick, O. Toader, P. Weng, N. A. Samad, Z. Jiao and G. S. Was: J. Nucl. Mater. **451** (2014) 40–47.
14) S. Lapuerta, N. Millard-Pinard, N. Moncoffre, N. Bererd, H. Jaffrezic, G. Brunel, D. Crusset and Th. Mennecart: Surf. Coat. Technol. **201** (2007) 8197–8201.
15) S. Lozano-Perez, K. Kruska, I. Iyengar, T. Terachi and T. Yamada: Corros. Sci. **56** (2012) 78–85.
16) S. J. Zinkle, P. J. Masiasz and R. E. Stoller: J. Nucl. Mater. **206** (1993) 266–286.